

Spatially Correlated Blockage Aware Placement of RIS in IIoT Networks

Rashmi Kumari, Gourab Ghatak, and Abhishek K. Gupta .

Abstract—We study the impact of deploying reconfigurable intelligent surfaces (RISs) in mitigating coverage gaps and enhancing transmission reliability in an industrial internet of things (IIoT) network. First, we consider a single blockage scenario and characterize the correlation between blocking events of the base station (BS)-user and the RIS-user links and study its impact on the probability of establishing a viable reflected link. Then, by considering multiple blockages, we derive the distribution of the signal to noise ratio (SNR) as a function of data size, blockage density, the number of RISs, and the deployment area. We analyze the impact of normalized blockage radius and identify the threshold beyond which the assumption of independent blockages deviates from the ground truth of correlated blocking. Finally, we compare the outage performance of this RIS-assisted system with that operated with network-controlled relays, and demonstrate that while the relays provide a higher reliability beyond a certain blockage threshold, increasing the number of RISs may help mitigate this effect. These insights offer valuable design guidelines for deploying RIS-aided IIoT networks in dense blockage environments.

I. INTRODUCTION

Traditionally, wired communication, such as Ethernet, is common in industrial automation and monitoring setups. However, with increasing scale, it can be costly to install and maintain [1]. To improve deployment flexibility and reduce costs, industries are transitioning towards wireless systems [2]. Future industrial wireless networks will include various devices that demand high communication reliability and low latency [3]. To meet these requirements, especially for time-sensitive control applications, ultra-reliable low-latency communications (URLLCs) are essential in fifth generation (5G), prioritizing latency, dependability, and availability [4]. Additionally, massive connectivity presents challenges regarding coverage and capacity, which are addressed by protocols such as those suggested by Shah *et al.* [5]. However, unfavorable channel conditions due to the presence of physical blockages in the factory can weaken the power of wireless signals, degrading the quality of service (QoS) for such applications [6]. This effect is more prominent at high frequencies, including millimeter wave (mm-wave) bands. To address this, Swamy

et al. [7] suggested multi-hop transmission with cooperative relaying, where stronger devices help those with weaker channels. The authors in [8] extended this by evaluating the protocol in settings with random blockages. While dedicated relays can improve network performance, their high installation costs and the complexity of optimized placement make them less practical. Instead, the study proposes leveraging existing network devices as relays, offering a scalable solution adaptable to any network size.

The deployment of Reconfigurable intelligent surfaces (RIS) have emerged as a promising approach to mitigate blockage-effects by dynamically altering the signal propagation with tunable signal reflections [9]. This potentially improves coverage by providing alternate signal paths when direct links are blocked, thus mitigating blockage effects. While prior research has mainly focused on electromagnetic characterization, physical modeling, and performance assessment in simplified networks, several studies have explored deploying RISs near transmitters or receivers to boost signal power. However, a close proximity of the RIS to either the transmitters or the receivers may lead to a joint obstruction of the links due to correlated blocking. Consequently, simultaneous blocking of transmitter-receiver and RIS-receiver paths can disrupt communication. Since blockages can affect multiple links simultaneously, leading to correlation among link blockages, it is important to study its impact on the performance of a wireless industrial internet of things (IIoT) network with RIS to determine the optimal placement of RISs in such a network. This paper investigates the impact of uniformly distributed RISs in IIoT networks under correlated blocking, focusing on addressing coverage gaps and enhancing transmission reliability in industrial applications.

A. Related Work

On solutions to augment reliability in IIoT Networks:

To improve the reliability of IIoT networks, researchers have investigated strategies such as diversity techniques, relaying, and cooperative transmission [3], [7]. The authors in [3] have considered latency-constrained services and have proposed transmission techniques that dynamically adapt to the requirements. Whereas, the authors in [7] have demonstrated that cooperative transmission using multiple devices can lead to a high degree of reliability even in a low or moderate signal to noise ratio (SNR) regime. An interesting aspect of their study is the revelation that under realistic channel conditions, merely a frequency diversity scheme is insufficient to achieve an error rate corresponding to high-reliability applications.

R. Kumari and G. Ghatak are with the Department of Electrical Engineering, Indian Institute of Technology Delhi, India 110016. Email: {eez228188, gghatak}@ee.iitd.ac.in. A. K. Gupta is with the Department of Electrical Engineering, Indian Institute of Technology Kanpur, India 208016. Email: gkrabhi@iitk.ac.in. The work is supported in part by Qualcomm 6GUR and DST SERB grant

A preliminary version of this paper has been accepted for presentation at the IEEE International Symposium on Personal, Indoor and Mobile Radio Communications (PIMRC), 2025.

Their proposed scheme selects a transmission rate that is characterized by the channel condition of the worst device. On the contrary, the work by Jurdi *et al.* [10] have proposed an adaptive rate selection scheme, where, first, the channel state information of the coordinating node to the edge devices is estimated. This is followed by an adaptation of the transmission rate for each node to its instantaneous channel state. However, such a solution leads to a massive overhead due to the estimation procedure of individual channels. The authors in [11] have shown that multiple antennas reduce the SNR required for decoding, improving the capacity and coverage of the network. The authors in [8] have demonstrated the reduction in the reliability of transmission with blockages and also evaluated the performance of multi-device cooperation schemes to alleviate the outage. However, similar to the other works on the topic, the author had largely ignored the medium access control (MAC) overhead associated with such a policy. This paper proposes strategic placement of RISs to fill coverage holes and enable high-reliability transmission for IIoT use cases.

Impact of Blockages: In an IIoT scenario, the blockages can have metallic bodies which cause a detrimental impact on signal coverage, even in lower-frequency transmissions [12], [13]. To understand the impact of blockages in such networks, stochastic geometry provides tools from random shape theory [14]. Moreover, in indoor scenarios, the links may be highly correlated due to the geometric structure of the blockages and their proximity to the transmitter and the user. Most works ignore this correlation and instead assume that blocking events for different links are independent, e.g., see the recent work [15]. The work [16] showed that spatially correlated blockages can significantly impact signal to interference plus noise ratio (SINR), highlighting the need to model such effects. The impact of correlated blockages has been analyzed in 1D RIS-assisted networks [17] and 2D mm-wave networks [16], [18]. The empirical SINR was calculated in [19] using a correlation model for fixed blockages, while [20] studied blockage correlation for sensor localization. The authors in [21] investigated the time correlation of blocking events due to user mobility at two-time instants, and [22] studied interference correlations, though simultaneous base station (BS) blockage effects were not considered.

RIS placement strategies: Initial studies on RISs have focused on physical modeling, electromagnetic characterization, and simple network performance evaluation [23]. Since the path loss of the transmitter to the receiver link via the RIS varies as the product of the path losses of the individual (i.e., transmitter to the RIS and the RIS to the receiver) links, the deployment of the RIS close to the transmitter or the receiver maximizes the received signal power [24]. However, such a deployment strategy may result in the transmitter-receiver and the RIS-receiver links being blocked simultaneously, resulting in a high service outage. A comparison between dispersed RISs and relays in single input single output (SISO) systems, where users connect to the device offering the highest SNR, has revealed that RISs outperform relays in energy efficiency and outage probability, especially with dense deployment or high element counts [25]. For outdoor networks, widespread

RIS placement minimizes blind spots [26]. In dense environments like malls or airports, smaller, distributed RISs provide superior coverage [27], while industrial settings often integrate RISs on walls to enhance coverage [28]. The correlation in placements of blockages also plays a significant role in determining optimal RIS locations in the presence of blockages, e.g., [17] have derived correlation-aware RIS placement strategies for outdoor mm-wave networks. Despite their importance, the impact of indoor blockages and corresponding correlation in industrial settings remains underexplored, highlighting the lack of a comprehensive methodology for accurately analyzing RIS performance under correlated blockage conditions.

B. Contributions and Organization

We examine the performance gains offered by the use of RISs in an IIoT network inside a warehouse to address coverage gaps and improve transmission reliability by taking into account the correlation among the blockages of the links involved. The key contributions of this work are summarized as follows.

- 1) We demonstrate how uniformly deployed RISs on the periphery of the warehouse can effectively mitigate blind spots caused by random blockages and enhance transmission reliability. For this, we consider the BS-user link as a cascade of the direct and via-RIS links and characterize its line of sight (LoS) probability by considering the correlation between blocking events of these two links. Specifically, we develop analytical methods to characterize the correlation between blocking events of the BS-RIS link and the RIS-user link while determining the LoS probability of the via-RIS link between the BS and the user. This analysis reveals the conditions under which a viable reflected link can be established.
- 2) We extend the analysis to networks with multiple RISs by considering the correlation between the blockages of the BS-RIS and RIS-user links for each individual RIS, while considering independent blocking across different RISs. We derive closed-form expressions for the LoS/non line-of-sight (NLoS) probabilities and validate them using Monte-Carlo simulations, highlighting the influence of blockage size, location, and user position on link availability.
- 3) Leveraging the derived LoS probability, we derive the outage probability of a uniformly located user in the network. We analyze the impact of the target rate, blockage size, and blockage distance on the outage probability and identify conditions under which a given URLLC QoS requirement in terms of reliable delivery of a fixed payload with minimal latency can be guaranteed. Additionally, we analyze the impact of the normalized blockage size and identify the point beyond which the performance under the independent blockage assumption begins to deviate noticeably from correlation-aware models, highlighting the limitations of assuming independence in environments with larger blockages. More importantly, we highlight the importance of strategic and user-centric placement of RIS such that it creates

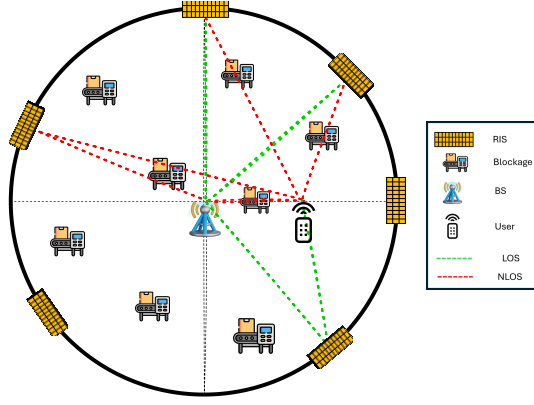


Fig. 1. System Model

new paths to user and BS with mutually uncorrelated blocking events.

- 4) Finally, using simulations, we show that beyond a certain number of blockages, a network-controlled relay or repeater can outperform a single RIS deployment in terms of reducing outage probability. Our analysis shows that deploying multiple RISs can surpass the outage performance of a network-controlled relay, offering a scalable solution for enhancing reliability under severe blockage conditions. To determine the number of RISs needed to effectively address coverage gaps and enhance transmission reliability in IIoT networks, we derive the corresponding SNR-based rate coverage probability for the user. Additionally, we examine the impact of warehouse radius and the number of RISs on outage probability under various blockage conditions. These insights provide valuable guidance for deploying RIS-aided URLLC wireless communication networks in IIoT environments.

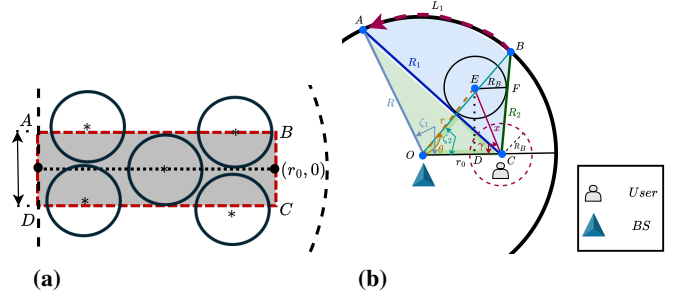
The rest of the paper is organized as follows. In Section II, we introduce the system model for the RIS-assisted factory environment, discuss the deployment of the RISs, characterize the blockage process, and outline the path loss model. Section III covers the derivation of the probability that the link between the RIS-BS and the user is in NLoS, while Section IV covers the derivation of SNR and rate coverage probability of the user. We discuss the numerical and simulation results in Section V. Finally, Section VI concludes this paper by examining the number of RISs needed to surpass the performance of relays.

II. SYSTEM MODEL

A. Network Geometry

We consider an IIoT network with a BS placed at the center of a warehouse shaped like a circular disk with radius R . Let us consider a user located at a distance of r_0 along the positive x-axis¹, as illustrated in Fig. 1. Due to dynamic blockages, the link between the BS and the user can either be in LoS or NLoS. Assume n_R RISs, each equipped with M passively reflecting elements, uniformly deployed on the inner wall at

¹We assume that $r_0 \geq 2R_B$ since if the user is closer to the BS, it is unlikely that the BS-user link is blocked.

Fig. 2. An illustration showing (a) the direct link blockage and (b) the range where RIS is blocked from the user given a blockage at E

the boundary of the room. Let the location of the i^{th} RIS be denoted by \mathbf{z}_i , where $i = 1, 2, \dots, n_R$.

Blockages. Let n_B blockages be located at $\{\mathbf{y}_j = r_j \angle \theta_j\}_{j=1}^{n_B}$ within the circular room such that their distances from the center is uniform and independent across blockages. Each blockage is modeled as a disk of radius R_B . Their positions relative to the origin are given by $(r \cos \theta, r \sin \theta)$, where $r \sim \mathcal{U}(R_B, R - R_B)$ and $\theta \sim \mathcal{U}(0, 2\pi)$, where $\mathcal{U}(a, b)$ denotes the uniform distribution between a and b . Although the blockages are modeled as circular disks, they are allowed to overlap in this work, offering a more realistic representation of industrial environments where blockages may intersect.

SNR model for the direct link. The direct received power P_D at the user from the BS is $P_D = P h_D K r_0^{-\alpha_1}$, where r_0 is the distance of the user from the BS, h_D denotes the fading power gain on the direct link. We assume Rayleigh fading in the direct link which implies that h_D is exponentially distributed.

SNR model for the indirect links. The indirect links are the cascaded links from the BS to the RISs and subsequently from the RISs to the user. The indirect received power P_{I_i} is [29]

$$P_{I_i} = P K M^2 \sum_{i=1}^{n_R} h_{I_i} (\ell(r_0, \phi_i) R)^{-\alpha_1}, \quad (1)$$

where $\ell(r_0, \phi_i)$ represents the distance from the user to the i^{th} RIS, R denotes the distance from the RISs to the BS, and M is the total number of RIS elements. The indirect link fading is assumed to be Nakagami- m distributed with shape parameter m and spread parameter Ω , which accurately captures a wide range of propagation conditions and is widely adopted in the RIS literature for analytical tractability [30]. As per Alzer's lemma [12], the complementary cumulative density function (CCDF) of h_I is upper-bounded as $F_{h_I}(x) \leq \sum_{n=1}^m (-1)^{n+1} \binom{m}{n} e^{-nx\eta}$, with $\eta = m(m!)^{-\frac{1}{m}}$. Before proceeding with the analysis of the indirect link, we first recall that the blockage probability of the direct link (let us call it event E_0) can be derived using the void probability of a binomial point process (BPP). As illustrated in Fig. 2(a), a link obstruction occurs when the center of at least one blockage lies within the shaded region $(ABCD)^2$, which has dimensions

²Note that the actual blockage region is a capsule shape consisting of a rectangle of area $2R_B r_0$ and two half-circles of total area πR_B^2 . For analytical simplicity, the circular cap area is neglected, which is valid when $R_B \ll r_0$ and $R_B \ll R$.

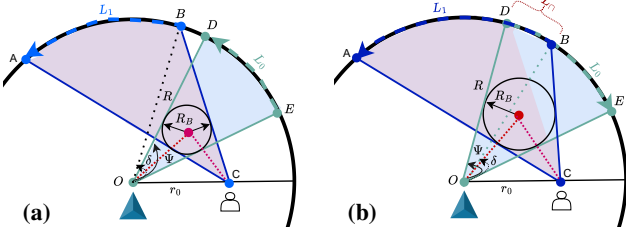


Fig. 3. An illustration showing the RIS location range that may result in blocking of RIS-BS and RIS-User link for given blockage for two cases.

$r_0 \times 2R_B$.

$$\mathbb{P}(E_0) = q_B(r_0) = 1 - \left(1 - \frac{2r_0 R_B}{\pi R^2}\right)^{n_B}.$$

III. BLOCKAGE PROBABILITY OF THE INDIRECT LINK

A blockage in the signal path between a user and an RIS can disrupt BS-RIS and RIS-user connections, depending on their relative location and blockage size, leading to a correlation in blocking of these links. To highlight the correlation in these links, we first consider the case of a single blockage before extending to the multiple blockages scenario.

A. Blocking Correlation for Single Blockage

Let us consider a blockage located at E at location $\mathbf{y} = r\angle\theta$ (See Fig. 2(b)).

1) *Blockage of RIS-user link:* Let the RIS be located uniformly anywhere on the boundary. Let Z_{R_1U} denote the link between the RIS and the user. Let B_{R_1U} represent the event that Z_c is blocked which occurs when the RIS is inside the arc AB where AB is the projection of the blockage at the boundary from the user (see Fig. 2(b)) with its length L_1 given in the following Lemma.

Lemma 1. The length L_1 of AB is

$$L_1 = \begin{cases} 2\pi R, & \text{if } (r^2 - 2rr_0 \cos \theta) \leq R_B^2 - r_0^2, \\ R \left(\arcsin \left(\frac{r_0 \sin \gamma_2}{R} \right) - \arcsin \left(\frac{r_0 \sin \gamma_1}{R} \right) + \chi \right), & \text{o.w.,} \end{cases} \quad (2)$$

where $\gamma_1 = \gamma - \frac{\chi}{2}$, $\gamma_2 = \gamma + \frac{\chi}{2}$,

with $\gamma = \arcsin \left(\frac{r \sin \theta}{\sqrt{(r \sin \theta)^2 + (r_0 - r \cos \theta)^2}} \right)$,

and $\chi = 2 \arcsin \left(\frac{R_B}{\sqrt{(r \sin \theta)^2 + (r_0 - r \cos \theta)^2}} \right)$.

Proof: From Fig. 2(b), the arc length $L_1 = R(\zeta_1 - \zeta_2)$. In $\triangle CDE$, $\angle D = \frac{\pi}{2}$, $CD = r_0 - r \cos \theta$, and $ED = r \sin \theta$. Accordingly, $x \triangleq CE = \sqrt{(r \sin \theta)^2 + (r_0 - r \cos \theta)^2}$. Further, $\gamma \triangleq \angle ECD = \arcsin \left(\frac{r \sin \theta}{x} \right)$. In triangle $\triangle ECF$, $\angle ECF$ is $\frac{\chi}{2}$, where Let $\chi \triangleq 2\angle ECF = 2 \arcsin \left(\frac{R_B}{x} \right)$. Let γ_1 and γ_2 denote $\angle ACO$ and $\angle BCO$. Applying the sine rule in triangles $\triangle AOC$ and $\triangle BOC$ respectively yields

$$\begin{aligned} \zeta_1 &= \pi - \arcsin \left(\frac{r_0 \sin(\gamma_1)}{R} \right) - \gamma_1, \\ \text{and } \zeta_2 &= \pi - \arcsin \left(\frac{r_0 \sin(\gamma_2)}{R} \right) - \gamma_2. \end{aligned} \quad (3)$$

Thus, the arc length L_1 simplifies to (2). ■

2) *Blockage of RIS-BS link:* Similarly, the event B_{BR_1} that the link Z_{BR_1} between the RIS and the BS is blocked, corresponds to RIS being inside DE . Here, DE is the projection of the blockage at the boundary from the BS with its length L_{01} , obtained by substituting $r_0 = 0$ in L_1 , given as

$$L_{01} = R\chi_2, \quad (4)$$

where $\chi_2 = 2 \arcsin \left(\frac{R_B}{r} \right)$.

3) *Blockage of cascade link:* The cascade indirect link is blocked if both the BS-RIS and RIS-user links are blocked simultaneously, i.e., $B_{BR_1} \cup B_{R_1U}$. However, B_{BR_1} and B_{R_1U} are correlated, since the same blockage object can obstruct both links, making the computation of the joint blocking probability non-trivial. Here, blockage correlation refers to the statistical dependence between the blocking events of the BS-RISs and RISs-user links, following the discussion in [18]. In fact, the event $B_{BR_1} \cap B_{R_1U}$, where both links are blocked, corresponds to the case that RIS lies inside the intersection of AB and DE . Its length $L_{\cap 1}$ depends on whether the arcs AB and DE overlap. Let $\Psi = \theta + \frac{\chi_2}{2}$ and $\delta = \zeta_2$. If $\delta \geq \Psi$, the arcs do not intersect (see Fig. 3(a)), otherwise the arcs intersect (See Fig. 3(b)). Therefore,

$$L_{\cap 1} = \begin{cases} 0 & \text{if } \delta \geq \Psi, \\ R \left(\theta + \frac{\chi_2}{2} - \zeta_2 \right) & \text{otherwise,} \end{cases} \quad (5)$$

Now, note that the cascade (via-RIS) indirect link Z_{BR_1U} is NLoS if any of the two links Z_{BR_1} or Z_{R_1U} is blocked i.e. $B_{R_1U} \cup B_{BR_1}$. Assuming the RIS location is uniformly distributed on the boundary, we get the following result.

Lemma 2. Given a blockage at $\mathbf{y} = r\angle\theta$, the probabilities that the link Z_{BR_1} , the link Z_{R_1U} and the cascade indirect link Z_{BR_1U} is blocked, are respectively given as

$$\mathcal{P}_{R_1U}(r, \theta) = \frac{L_1}{2\pi R}, \quad \mathcal{P}_{BR_1}(r, \theta) = \frac{L_{01}}{2\pi R}, \quad (6)$$

$$\mathcal{P}_{BR_1U}(r, \theta) = \mathbb{P}(B_{R_1U} \cup B_{BR_1}) = \frac{L_1 + L_{01} - L_{\cap 1}}{2\pi R}. \quad (7)$$

Proof: Lemma 2 can be derived from Lemma 1, together with (4) and (5). ■

Remark 1. $L_{\cap 1}$ captures the correlation in the BS-RIS and the RIS-user links which is generally ignored in existing literature.

Corollary 1. For a blockage located at $\mathbf{y} = r\angle\theta$ and n_R RISs, the probability that the cascade indirect link Z_{BRU} is blocked is given as

$$\mathcal{P}_{BRU}(r, \theta) = \prod_{i=1}^{n_R} \mathbb{P}(B_{R_iU} \cup B_{BR_i}) = \prod_{i=1}^{n_R} \left(\frac{L_i + L_{0i} - L_{\cap i}}{2\pi R} \right), \quad (8)$$

where $i = 1, 2, \dots, n_R$. Here L_i , L_{0i} and $L_{\cap i}$ denotes the effective blockage lengths associated with the RIS-user, BS-RIS, and their intersection for the i^{th} RIS, respectively. Note that for each RIS, the BS-RIS and RIS-user links are correlated, while signals from different RISs are assumed independent.

B. User-RIS Link Visibility With Multiple Blockages

To analyze the case with multiple blockages, we condition on the location of the RIS and study the statistics across random realizations of the blockage process. As per Fig. 4(a), let an RIS be located at point F at an angle ϕ from the origin O . The user is at $E := (r_0, 0)$. A single blockage can be approximated by a line segment of length $2R_B$ acting as its projection. Accordingly, line segments of length R_B are drawn from the user towards points A and B , and from the RIS towards points C and D , forming the rectangle $ABCD$ ³. The RIS-user link is blocked if the center of a blockage lies within this rectangle. However, since a portion of $ABCD$ extends beyond the room where blockages cannot exist. The effective region of interest is the intersection region denoted by $ABGFD$, where the blockages should not lie. Its area A_{ABGFD} needs to be calculated explicitly.

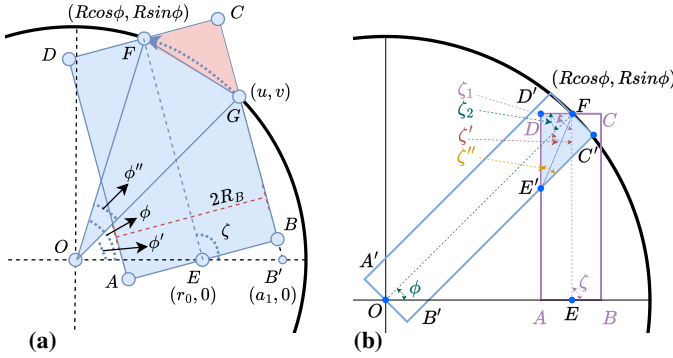


Fig. 4. Illustration showing the region where blockages should not fall to ensure the visibility of (a) RIS-User and (b) RIS-BS and RIS-User.

Lemma 3. *Given that the RIS is at an angle ϕ , the probability $\mathcal{P}_{n_B}(r_0, \phi)$ that the user-RIS link is blocked is*

$$q_{R_1U} = \mathcal{P}_{n_B}(r_0, \phi) = 1 - \left(1 - \frac{A_{ABGFD}}{\pi R^2}\right)^{n_B} \quad (9)$$

where $A_{ABGFD} =$

$$2R_B \ell_1 - \left(\frac{R^2 \sin^2 \phi''}{2} + \frac{R_B(\ell_1 - z_1 + R_B/m_1)}{2} - \frac{\phi'' R^2}{2}\right).$$

with $\ell_1 = \sqrt{(R \cos \phi - r_0)^2 + R^2 \sin^2 \phi}$ and $z_1 = \sqrt{v^2 + (u - a_1)^2}$, with $u = \frac{m_1^2 a_1 + \sqrt{R^2(1+m_1^2) - m_1^2 a_1^2}}{1+m_1^2}$, $v = m_1(u - a_1)$, $m_1 = \frac{R \sin \phi}{R \cos \phi - r_0}$, $a_1 = \frac{R_B}{m_1} \sqrt{(m_1^2 + 1)} + r_0$, and $\phi'' = \phi - \arcsin\left(\frac{z_1}{R}(\pi - \arctan(m_1))\right)$.

Proof: We calculate the area of $ABGFD$ by subtracting the area of $\triangle FCG$ and the area of the segment OFG from the area of the square $ABCD$. For this, we first derive the area of the triangles $\triangle FOG$, $\triangle FCG$, and sector FOG , as shown in Fig. 4(a). The equation of line FE is $y = m_1(x - r_0)$, where

$m_1 = \frac{R \sin \phi}{R \cos \phi - r_0}$. The distance between points F and E , denoted by ℓ_1 , is $\ell_1 = \sqrt{(R \cos \phi - r_0)^2 + R^2 \sin^2 \phi}$. The distance between E and B is $R_B = m_1 \frac{|a_1 - r_0|}{\sqrt{m_1^2 + 1}}$. The coordinate of $(a_1, 0)$, where line CB intersects the positive x -axis at point B' , is $a_1 = \frac{R_B}{m_1} \sqrt{(m_1^2 + 1)} + r_0$. Similarly, the equation of line CB is $y_1 = m_1(x - a_1)$. The coordinates of point $G(u, v)$, where line CB intersects the disk of radius R centered at $(0, 0)$, are $G\left(\frac{m_1^2 a_1 + \sqrt{R^2(1+m_1^2) - m_1^2 a_1^2}}{(1+m_1^2)}, m_1(u - a_1)\right)$. Let z_1 be the distance between points G and B' , given by $z_1 = \sqrt{v^2 + (u - a_1)^2}$. Using the Sine rule in $\triangle GOB'$, $\phi' = \arcsin\left(\frac{z_1}{R}(\pi - \zeta)\right)$. The angle of sector FOG is $\phi'' = \phi - \phi'$, and the length FG is $R\phi''$. Thus, the area of sector FOG is $A_{FOG} = \left(\frac{\phi'' R^2}{2}\right)$. The sides of $\triangle FOG$ are $FO = R$, $OG = R$, and the included angle $\angle FOG = \phi''$, then the area of $\triangle FOG$ is $A_{\triangle FOG} = \frac{R^2 \sin \phi''}{2}$. The area of the right triangle $\triangle FCG$, with base $FC = R_B$ and height $CG = \ell_1 - \left(z_1 + \frac{R_B}{m_1}\right)$ is $A_{\triangle FCG} = \frac{R_B(\ell_1 - (z_1 + \frac{R_B}{m_1}))}{2}$. The area of the polygon $ABGFD$ is obtained by subtracting the area of $\triangle FCG$ the rectangle $ABCD$, given by $A_{ABCD} = 2R_B \ell_1$, as shown in Fig. 4(a). Adding the area of sector minus $\triangle FOG$ into it, we get the desired result. ■

Similarly, given that the RIS is at an angle ϕ , the probability that the BS-RIS link is blocked is given as

$$q_{BR_1} = \left(1 - \frac{2R_B R - 2\left(\frac{R^2 \sin \phi'}{2} + \frac{R_B(\ell_1 - (z_2 + \frac{R_B}{m_2}))}{2} - \frac{\phi'_1 R^2}{2}\right)}{\pi R^2}\right)^{n_B} \quad (10)$$

where $z_2 = \sqrt{v_1^2 + (u_1 - a_2)^2}$, $v_1 = m_2(u_1 - a_2)$, $u_1 = \frac{m_2^2 a_2 + \sqrt{R^2(1+m_2^2) - m_2^2 a_2^2}}{1+m_2^2}$, $m_2 = \tan \phi$, and $a_2 = \frac{R_B}{m_2} \sqrt{(m_2^2 + 1)}$. Also, $\phi'_1 = \phi - \phi_1$, where $\phi_1 = \arccos\left(\frac{2Ra_2}{R^2 + a_2^2 - z_2^2}\right)$. This result can be obtained easily by substituting $r_0 = 0$ in Lemma 3.

C. Visibility of Cascade User-RIS-BS Link Under Multiple Blockages

Next, we see that the shaded region $AEB'E'$ represents the intersection between the RIS-user link, shown in Fig. 4(b). Hence, the probability that Z_{R_1U} and Z_{BR_1} are blocked simultaneously is $\mathbb{P}(Z_{R_1U} \cap Z_{BR_1}) = 1 - \left(1 - \frac{A_{FDC'E'}}{\pi R^2}\right)^{n_B}$. Therefore, the probability that the cascade indirect (via-RIS) link is blocked (*i.e.* at least one of the BS to RIS link and the RIS to user link is blocked) is given as

$$\mathbb{P}(Z_{R_1U} \cup Z_{BR_1}) = q_{R_1U} + q_{BR_1} - 1 + \left(1 - \frac{A_{FDC'E'}}{\pi R^2}\right)^{n_B}$$

Theorem 1. *The probability that the cascaded indirect (via-RIS) link is blocked, is given as*

$$q_{BR_1U} = \mathbb{P}(Z_{R_1U} \cup Z_{BR_1}) = q_{R_1U} + q_{BR_1} \quad (11)$$

³The actual geometry would be a rounded rectangle, which is approximated by a rectangle for analytical tractability. In the numerical results section, we will show that this approximation does not affect the key insights.

$$-1 + \left(1 - \frac{1}{\pi R^2} \left(\frac{R_B^2}{\tan(\frac{\zeta''}{2})}\right)\right)^{n_B}, \quad (12)$$

where $\zeta'' = \arctan\left(\frac{R \sin \phi}{R \cos \phi - r_0}\right) - \phi$.

Proof: In the quadrilateral $DFC'E'$, we have $\angle D = \angle C' = \pi/2$ and $\angle F + \angle E' = \pi$. Given $DF = FC' = R_B$, two adjacent sides are equal, and one opposite angle is right, classifying $DFC'E'$ as a kite. To validate this, drawing a bisector from F to E' shows that triangles $\triangle FDE'$ and $\triangle FC'E'$ are congruent by the RHS criterion. Specifically, $\angle D = \angle C'$, both are right angles; $DE' = C'E'$, the adjacent sides are equal, and FE' is the common hypotenuse. Thus, $DFC'E'$ forms a kite, and $DE' = C'E'$. The kite's area is the sum of $\triangle FDE'$ and $\triangle FC'E'$. Let $\zeta' = \zeta_1 - \zeta_2$, where $\zeta_1 = \arctan(m_1)$ and $\zeta_2 = \arctan(m_2)$, with m_1 and m_2 as slopes of lines FE and FO , respectively. The side length DE' is $DE' = \frac{R_B}{\tan(\frac{\zeta''}{2})}$, where $\zeta'' = \zeta'$ by parallelogram properties.

Hence, the area of $\triangle FDE'$ is $(\frac{R_B^2}{2 \tan(\frac{\zeta''}{2})})$. Thus, the shaded region $FDC'E'$ area is

$$A_{FDC'E'} = \left(\frac{R_B^2}{\tan(\frac{\zeta''}{2})}\right).$$

D. Visibility of Cascade User-RISs-BS Links Under Multiple Blockages and Multiple RISs

As discussed in Theorem 1, the blockage events affecting the user-RIS and RIS-BS links can be fully correlated, i.e., if a blockage obstructs one of the two links, it is likely to obstruct the other as well. Further, for tractability in our analysis, the blockage events across different RISs are considered statistically independent, as the spatial separation between RISs leads to distinct propagation paths and non-overlapping blockage regions. This hybrid correlation model captures a realistic scenario where the joint blockage behavior within a single cascade link is preserved, while still allowing spatial diversity across multiple RISs to mitigate the risk of complete link outage. In Section V, we demonstrate with numerical results that this approach lends remarkable accuracy to the actual performance while maintaining a high degree of tractability. On the contrary, removing the correlation aspect in the individual RIS links results in a significant loss of accuracy.

Lemma 4. *Assuming that the blockage events across different RISs are statistically independent, the probability that all cascade links via the n_R RISs are simultaneously blocked is given by $q_{BR_1:n_R U} = \prod_{i=1}^{n_R} q_{BR_i U}$, where $q_{BR_i U}$ denotes the probability that the cascaded link via the i^{th} RIS is blocked and given as, $q_{BR_i U} = q_{R_i U} + q_{BR_i} - 1 + \left(1 - \frac{1}{\pi R^2} \left(\frac{R_B^2}{\tan(\frac{\zeta''}{2})}\right)\right)^{n_B}$. Here $q_{R_i U} = 1 - \left(1 - \frac{2R_B \ell_i - \left(\frac{R^2 \sin \phi'_i}{2} + \frac{R_B(\ell_i - z_i + R_B/m_i)}{2} \cdot \frac{\phi'_i R^2}{2}\right)}{\pi R^2}\right)^{n_B}$ and $q_{BR_i} = \left(1 - \frac{2R_B R - 2\left(\frac{R^2 \sin \phi'_i}{2} + \frac{R_B(\ell_i - (z_i + \frac{R_B}{m_i}))}{2} \cdot \frac{\phi'_i R^2}{2}\right)}{\pi R^2}\right)^{n_B}$.*

Proof: Similar to Theorem 1, which considers the case of $n_R = 1$, we can extend the result to multiple RISs. The probability that the cascade indirect link via the i^{th} RIS is blocked is given by

$$q_{BRU} = \mathbb{P}(Z_{R_i U} \cup Z_{BR_i}) = q_{R_i U} + q_{BR_i} - \mathbb{P}(Z_{R_i U} \cap Z_{BR_i})$$

where $q_{R_i U}$ and q_{BR_i} denote the probabilities that the links between the user and the i^{th} RIS, and between the BS and the i^{th} RIS, respectively, are blocked, as discussed in subsection III-B. ■

IV. SNR DISTRIBUTION

In this section, we calculate the SNR coverage probability for a test user located at a distance r_0 from the BS. We assume that the user receives the signal through reflections from only those RISs that are in LoS with both the user and the BS. The SNR is defined as $\text{SNR} = \frac{P_R}{N_0}$, where N_0 is the noise power and P_R denotes the received power at the user given by $P_R = \mathbb{I}_D P_D + \sum_{i=1}^{n_R} \mathbb{I}_{L_i} P_{L_i}$, where \mathbb{I}_D and \mathbb{I}_{L_i} are the indicator functions denoting the LoS availability of the direct and the i^{th} indirect links, respectively. The direct power is $P_D = PK h_D r_0^{-\alpha_1}$ while the reflected power is $P_{L_i} = PK M^2 \sum_{i=1}^{n_R} h_{L_i} (\ell(r_0, \phi_i) R)^{-\alpha_1}$. Based on the visibility state (LoS vs NLoS) of the direct link, there will be only two cases: one with the direct link in LoS and the other with the direct link in NLoS. The communication link is considered successfully covered when $\text{SNR} \geq \gamma_{\text{th}}$, where γ_{th} is the minimum SNR threshold required for the target application. It is given by $\gamma_{\text{th}} = 2^{\frac{b}{\beta T W}}$, where b is the data size in bits, β is the time partitioning factor (assumed $\beta = 1$), T is the transmission time, and W is the bandwidth [8]. The SNR coverage probability for a user located at a distance r_0 from the BS is

$$\mathcal{P}_C(r_0, \phi_i) = \mathcal{P}_{C_1}(\gamma_{\text{th}}|r_0)(1 - q_B(r_0)) + \mathcal{P}_{C_2}(\gamma_{\text{th}}|r_0)q_B(r_0), \quad (13)$$

where $\mathcal{P}_{C_1}(\gamma_{\text{th}}|r_0)$ denotes the conditional SNR coverage probability for the case when the direct link is in LoS, and $\mathcal{P}_{C_2}(\gamma_{\text{th}}|r_0)$ represents the conditional SNR coverage probability for the case when the direct link is in NLoS. Here, $q_B(r_0)$ denotes the probability that the direct link is in NLoS. The constraint $\text{SNR} \geq \gamma_{\text{th}}$ is equivalent to

$$\mathbb{I}_D P_D \geq \gamma_{\text{th}} N_0 - PK M^2 \sum_{i=1}^{n_R} h_{L_i} (\ell(r_0, \phi_i) R)^{-\alpha_1} \mathbb{I}_{L_i}, \quad (14)$$

where $\ell(r_0, \phi_i) = \sqrt{(R \cos \phi_i - r_0)^2 + R^2 \sin^2 \phi_i}$ denotes the distance between the user and the i^{th} RIS.

A. SNR in the presence of LoS Direct Link

First, let us condition on the event $\mathbb{I}_D = 1$ for a given r_0 ; then (14) can be modified as

$$P_D \geq \gamma_{\text{th}} N_0 - PK M^2 \sum_{i=1}^{n_R} h_{L_i} (\ell(r_0, \phi_i) R)^{-\alpha_1} \mathbb{I}_{L_i}. \quad (15)$$

Let the right-hand side of (15) be denoted by $\mathcal{T} = \gamma_{\text{th}} N_0 - PKM^2 \sum_{i=1}^{n_R} h_{I_i}(\ell(r_0, \phi_i)R)^{-\alpha_1} \mathbb{I}_{L_i}$. In order to characterize the SNR coverage probability, first we derive the Laplace transform (LT) of \mathcal{T} .

Lemma 5. For a given r_0 , the LT of \mathcal{T} is

$$\mathcal{B}_{\mathcal{T}}(s) = e^{-N_0 \gamma_{\text{th}} s} \times \left(\int_0^{2\pi} \left(1 - \frac{sPKM^2(\ell(r_0, \phi)R)^{-\alpha_1} \Omega}{m} \right)^{-m} \frac{\mathcal{P}_L(r_0, \phi)}{2\pi} d\phi \right)^{n_R} \quad (16)$$

where $\mathcal{P}_L(r_0, \phi)$ represents the probability that the indirect link between the BS, an RIS, and the user is in LoS, and is given by $\mathcal{P}_L(r_0, \phi) = (1 - q_{\text{BR}_1 \text{U}}(r_0, \phi))$.

Proof: The LT $\mathcal{B}_{\mathcal{T}}(s)$ of \mathcal{T} can be expressed as the product of the corresponding transforms of the noise power N_0 (which is a constant) and the reflected signal power, as follows

$$\begin{aligned} \mathcal{B}_{\mathcal{T}}(s) &= \mathbb{E} \left[e^{-s\gamma_{\text{th}} N_0} \exp \left(sPKM^2 \sum_{i=1}^{n_R} h_{I_i}(\ell(r_0, \phi_i)R)^{-\alpha_1} \mathbb{I}_{L_i} \right) \right] \\ &= e^{-N_0 s \gamma_{\text{th}}} \mathbb{E} \left[\exp \left(sPKM^2 \sum_{i=1}^{n_R} h_{I_i}(\ell(r_0, \phi_i)R)^{-\alpha_1} \mathbb{I}_{L_i} \right) \right] \\ &= e^{-N_0 s \gamma_{\text{th}}} \mathbb{E} \left[\prod_{i=1}^{n_R} e^{(sPKM^2 h_{I_i}(\ell(r_0, \phi_i)R)^{-\alpha_1} \mathbb{I}_{L_i})} \right] \\ &= \mathcal{B}_{N_0}(s \gamma_{\text{th}}) \mathcal{B}_{P_1}(s), \end{aligned} \quad (17)$$

where $\mathcal{B}_{N_0}(s \gamma_{\text{th}}) = e^{-N_0 s \gamma_{\text{th}}}$ and $\mathcal{B}_{P_1}(s) = \mathbb{E} \left[\prod_{i=1}^{n_R} e^{(sPKM^2 h_{I_i}(\ell(r_0, \phi_i)R)^{-\alpha_1} \mathbb{I}_{L_i})} \right]$. Further, $\mathcal{B}_{P_1}(s)$ can be simplified as

$$\begin{aligned} \mathcal{B}_{P_1}(s) &= \mathbb{E} \left[\prod_{i=1}^{n_R} e^{(sPKM^2 h_{I_i}(\ell(r_0, \phi_i)R)^{-\alpha_1} \mathbb{I}_{L_i})} \right], \\ &= \mathbb{E}_{\phi_i} \left[\prod_{i=1}^{n_R} \mathbb{E}_{h_{I_i}} \left[e^{(sPKM^2 h_{I_i}(\ell(r_0, \phi_i)R)^{-\alpha_1} \mathbb{I}_{L_i})} \right] \right]. \end{aligned} \quad (18)$$

Since $h_R \sim \text{Gamma}(m, \Omega/m)$, then the moment-generating function (MGF) of h_R is given by

$$\mathbb{E} [e^{u_i h_{I_i}}] = \left(1 - \frac{u_i \Omega}{m} \right)^{-m}, \quad \text{for } u_i < \frac{m}{\Omega}, \quad (19)$$

where $u_i = sPKM^2(\ell(r_0, \phi_i)R)^{-\alpha_1} \mathbb{I}_{L_i}$. Hence, (18) can be modified as

$$\begin{aligned} \mathcal{B}_{P_1}(s) &= \prod_{i=1}^{n_R} \mathbb{E}_{\phi_i} \left[\left(1 - \frac{sPKM^2(\ell(r_0, \phi_i)R)^{-\alpha_1} \Omega}{m} \right)^{-m} \right]. \\ \text{Hence, } \mathcal{B}_{\mathcal{T}}(s) &= e^{-N_0 s \gamma_{\text{th}}} \prod_{i=1}^{n_R} \mathbb{E}_{\phi_i} \left[\left(1 - \frac{sPKM^2(\ell(r_0, \phi_i)R)^{-\alpha_1} \Omega}{m} \right)^{-m} \right] \\ &= e^{-N_0 s \gamma_{\text{th}}} \left(\int_0^{2\pi} \left(1 - \frac{u\Omega}{m} \right)^{-m} \frac{\mathcal{P}_L(r_0, \phi)}{2\pi} d\phi \right)^{n_R}. \end{aligned} \quad (20)$$

We now compute the SNR coverage probability of the user

in the following two Theorems.

Theorem 2. The SNR coverage probability of the user located at a distance r_0 , when both the direct and reflected links are in LoS, is given by

$$\mathcal{P}_{c_1}(\gamma_{\text{th}}|r_0) = \mathcal{B}_{\mathcal{T}^+} \left(\frac{1}{KPr_0^{-\alpha_1}} \right), \quad (21)$$

where, $\mathcal{T}^+ \triangleq \max\{0, \mathcal{T}\}$.

Proof: The proof follows a similar approach to [31]. From definition,

$$\begin{aligned} \mathcal{P}_{c_1}(\gamma_{\text{th}}|r_0) &= \mathbb{P}(KPh_{\text{D}}r_0^{-\alpha_1} \geq \mathcal{T}|r_0), \\ &= \mathbb{P} \left(h_{\text{D}} \geq \frac{\mathcal{T}}{KPr_0^{-\alpha_1}} | r_0 \right). \end{aligned}$$

Note that

$$\mathbb{P} \left[h_{\text{D}} \geq \frac{\mathcal{T}}{KPr_0^{-\alpha_1}} | \mathcal{T}, r_0 \right] \stackrel{(a)}{=} \begin{cases} \exp \left(-\frac{\mathcal{T}}{KPr_0^{-\alpha_1}} \right) & \text{if } \mathcal{T} > 0, \\ 1 & \text{if } \mathcal{T} \leq 0, \end{cases}$$

where (a) follows from the CCDF of the exponential distribution. Let $f_{\mathcal{T}}(\cdot)$ denote the PDF of \mathcal{T} . Hence,

$$\begin{aligned} \mathcal{P}_{c_1}(\gamma_{\text{th}}|r_0) &= \int_0^{\infty} e^{-\frac{v}{KPr_0^{-\alpha_1}}} f_{\mathcal{T}}(x) dx + \int_{-\infty}^0 f_{\mathcal{T}}(x) dx, \\ &\stackrel{(b)}{=} \mathcal{B}_{\mathcal{T}^+} \left(\frac{1}{KPr_0^{-\alpha_1}} \right), \end{aligned} \quad (22)$$

where (b) follows from the definition of the LT of $\mathcal{B}_{\mathcal{T}^+}(s) = \int_{-\infty}^{\infty} e^{-s \max(t, 0)} f_{\mathcal{T}}(t) dt = \int_0^{\infty} e^{-sv} f_{\mathcal{T}}(x) dx + \int_{-\infty}^0 f_{\mathcal{T}}(x) dx$, evaluated at the argument $s = \frac{1}{KPr_0^{-\alpha_1}}$. ■

Note that $\mathcal{B}_{\mathcal{T}^+}(s)$ can be computed as

$$\mathcal{B}_{\mathcal{T}^+}(s) = \frac{1}{2\pi i} \int_{-\infty}^{\infty} \mathcal{B}_{\mathcal{T}}(s - iw) - \mathcal{B}_{\mathcal{T}}(-iw) \frac{dw}{w} + \frac{1 + \mathcal{B}_{\mathcal{T}}(s)}{2}. \quad (23)$$

The case when the direct link is in LoS and the reflected links are in NLoS can be seen as special case of Theorem 2 with $\mathbb{I}_{L_i} = 0, \forall i$. Here, (14) can be written as

$$P_{\text{D}} \geq \gamma_{\text{th}} N_0.$$

Hence, we get the following result.

Corollary 2. The SNR coverage probability for a test user located at a distance r_0 from the BS, when the direct link is in LoS and the reflected links are in NLoS is given by

$$\mathcal{P}'_{c_1}(\gamma_{\text{th}}|r_0) = e^{-\frac{\gamma_{\text{th}} N_0}{KPr_0^{-\alpha_1}}}. \quad (24)$$

Proof: This easily follows as shown below.

$$\begin{aligned} \mathcal{P}'_{c_1}(\gamma_{\text{th}}|r_0) &= \mathbb{P}(KPh_{\text{D}}r_0^{-\alpha_1} \geq \gamma_{\text{th}} N_0 | r_0), \\ &= \mathbb{P} \left(h_{\text{D}} \geq \frac{\gamma_{\text{th}} N_0}{KPr_0^{-\alpha_1}} | r_0 \right) = \exp \left(-\frac{\gamma_{\text{th}} N_0}{KPr_0^{-\alpha_1}} \right). \end{aligned} \quad \blacksquare$$

B. SNR in the absence of LoS Direct Link

Next, let us consider the case where $\mathbb{I}_D = 0$ for a given r_0 . Hence, (14) can be written as

$$\underbrace{PKM^2 \sum_{i=1}^{n_R} h_{L_i}(\ell(r_0, \phi_i)R)^{-\alpha_1} \mathbb{I}_{L_i}}_{X_{L_i}} \geq TN_0. \quad (25)$$

Theorem 3. The SNR coverage probability for the test user when the direct link is in NLoS, is

$$\mathcal{P}_{c_2}(\gamma_{th}|r_0) = \frac{1}{2} + \frac{1}{\pi} \int_0^\infty \frac{\text{Im}(e^{-it\gamma_{th}N_0} \varphi_L(t))}{t} dt, \quad (26)$$

$$\text{here } \varphi_L(t) = \left(\int_0^{2\pi} \left(1 - \frac{jtPKM^2(\ell(r_0, \phi)R)^{-\alpha_1}\Omega}{m} \right)^{-m} \frac{\mathcal{P}_L(r_0, \phi)}{2\pi} d\phi \right)^{n_R}.$$

Proof: The characteristic function of X_{L_i} is derived as follows:

$$\begin{aligned} \varphi_L(t) &= \mathbb{E}[e^{itX_{L_i}}] = \mathbb{E}\left[e^{itPKM^2 \sum_{i=1}^{n_R} h_{L_i}(\ell(r_0, \phi_i)R)^{-\alpha_1} \mathbb{I}_{L_i}}\right] \\ &= \mathbb{E}\left[\prod_{i=1}^{n_R} e^{itPKM^2 h_{L_i}(\ell(r_0, \phi_i)R)^{-\alpha_1} \mathbb{I}_{L_i}}\right] \\ &= \prod_{i=1}^{n_R} \mathbb{E}\left[e^{itPKM^2 h_{L_i}(\ell(r_0, \phi_i)R)^{-\alpha_1} \mathbb{I}_{L_i}}\right]. \end{aligned} \quad (27)$$

For a given r_0 , (27) be modified as

$$\begin{aligned} \varphi_L(t) &= \prod_{i=1}^{n_R} \mathbb{E}\left[\left(1 - \frac{jtPKM^2(\ell(r_0, \phi)R)^{-\alpha_1}\Omega}{m}\right)^{-m}\right] \\ &= \left(\int_0^{2\pi} \left(1 - \frac{jtPKM^2(\ell(r_0, \phi)R)^{-\alpha_1}\Omega}{m}\right)^{-m} \frac{\mathcal{P}_L(r_0, \phi)}{2\pi} d\phi\right)^{n_R}. \end{aligned} \quad (28)$$

We compute $\mathbb{P}(X_{L_i} \geq \gamma_{th}N_0) = 1 - \mathbb{P}(X_{L_i} \leq \gamma_{th}N_0)$ using the Gil-Pelaez inversion theorem [32], as derived in Theorem 3. ■

Therefore, based on Theorem 2 and Theorem 3, the SNR coverage probability for a test user located at a distance r_0 from the origin, within a circular warehouse of radius R , with a BS positioned at the origin and RISs deployed along the boundary wall at uniformly distributed azimuthal angles, is given by

$$\mathcal{P}_c(r_0) = \mathcal{P}_{c_1}(\gamma_{th}|r_0)(1 - q_B(r_0)) + \mathcal{P}_{c_2}(\gamma_{th}|r_0)q_B(r_0).$$

Hence the performance of the typical user randomly located in room is given as

$$\begin{aligned} \mathcal{P}_c &= E[\mathcal{P}_c(r_0)] \\ &= \frac{1}{R - 2R_B} \int_{R_B}^{R-R_B} \left(\mathcal{B}\tau^+ \left(\frac{1}{KP r_0^{-\alpha_1}} \right) (1 - q_B(r_0)) + \left(\frac{1}{2} + \frac{1}{\pi} \int_0^\infty \frac{\text{Im}(e^{-it\gamma_{th}N_0} \varphi_L(t))}{t} dt \right) q_B(r_0) \right) dr_0. \end{aligned} \quad (29)$$

The outage probability $\mathcal{P}_{out}(r_0, \phi_i)$ is derived from the coverage probability $\mathcal{P}_C(r_0, \phi_i)$ as

$$\mathcal{P}_{out}(r_0, \phi_i) = 1 - \mathcal{P}_C(r_0, \phi_i). \quad (30)$$

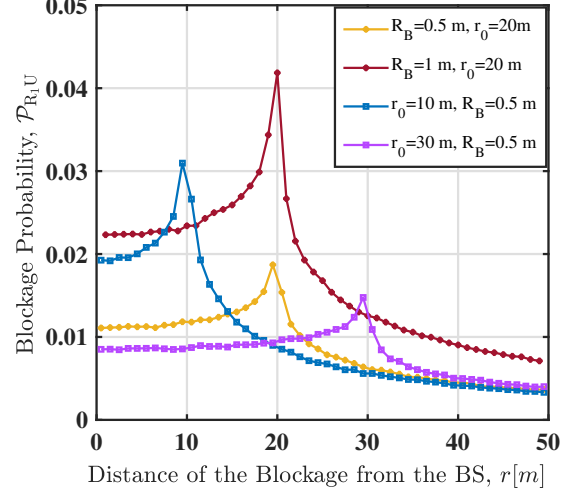


Fig. 5. $\mathcal{P}_{R_1U}(r_0, \theta)$ of blockage of RIS-user link, versus distance of the blockage from the BS, r . The first two plots show results for different blockage radii R_B with a fixed user location r_0 , while the remaining plots show results for different r_0 with a fixed R_B . Solid lines represent analytical expressions, while the markers represent simulation results.

As data size b increases, γ_{th} rises, leading to a higher outage. Blockages further degrade SNR and introduce variability, especially for nearby users. While RIS can mitigate this by establishing a LoS link, its effectiveness depends on its placement relative to the user and blockages.

V. NUMERICAL RESULTS AND DISCUSSION

This section presents numerical findings to illustrate the impact of different settings on the system's performance along with validating our analysis. The base station transmits with a power of 46 dBm⁴ and an antenna gain of 17 dBi. The warehouse radius is assumed to be either 100 m or 200 m. The carrier frequency is assumed to be 3.5 GHz with bandwidth of 1 MHz. The path loss constant is $K = \left(\frac{c}{4\pi f_c}\right)^2$, where c is the speed of light, and the path loss exponent is $\alpha_1 = 2$. The noise power is given by $N_0 = -174$ dBm/Hz, and the blockage radius R_B is assumed to be either 0.2 m or 0.5 m, as considered in [8].

A. Blockage Probability

Blockage probability between user and RIS in presence of single blockage: Fig. 5 illustrates the probability \mathcal{P}_{R_1U} that the user-RIS link is blocked as a function of blockage distance r , with $R = 50$ m for the case with single blockage as considered in Section III-A. The first two plots show how varying blockage radius R_B affects the blockage probability for a fixed user location $r_0 = 20$ m. When the blockage is near the BS and far from the user, the blockage probability is low. As the blockage moves outward to a radial distance comparable to the user's distance ($r \approx r_0$), the probability increases, peaking when the blockage has the highest chance

⁴Typical for large scale industrial applications that deploy macro cells rather than small cells for enterprise networks.

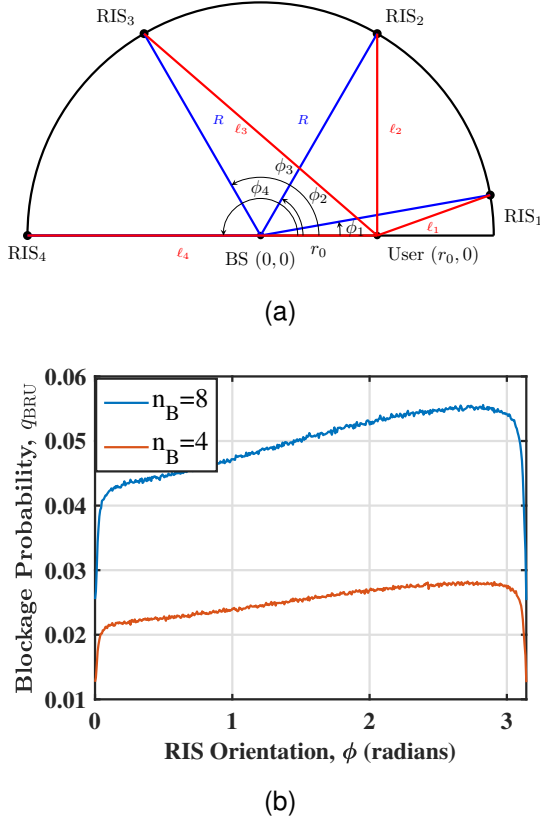


Fig. 6. (a) Variation of RIS-user path length (ℓ_i) with the orientation (ϕ_i) of the RISs. (b) Probability q_{BRU} that BS-RIS-user link is blocked versus the orientation of the RIS ϕ , for $R = 100$ m, $R_B = 0.2$ m, and $r_0 = 20$ m with multiple blockages.

of overlapping the direct path between the BS and the user. Beyond this point, the probability decreases as the blockage moves further away. A larger R_B raises the overall blockage probability across all distances. The last two plots show the effect of varying the user location r_0 for a fixed blockage radius $R_B = 0.5$ m. Here too, the blockage probability peaks when the blockage is near the user, with the peak shifting right as r_0 increases, indicating that the highest blockage probability aligns with the user's position relative to the BS.

Blockage probability of the cascade BS-RIS-user link: Fig. 6a shows the variation of the RIS-user path length ℓ_i with the RIS orientation angle ϕ_i . When ϕ_i is small, the RIS is closer to the user's direction, resulting in a shorter ℓ_i . As ϕ_i increases, the RIS moves farther around the semicircular boundary, which lengthens the RIS-user distance. Specifically, at $\phi = 0$, the path length is minimum, while at $\phi = \pi$, the RIS is located on the opposite side, and ℓ_i attains its maximum value. Thus, ℓ_i increases monotonically with ϕ_i . Fig. 6b shows the variation of correlated blockage probability for the BS-RIS-user link with RIS orientation angle ϕ , for $n_B = 4$ and $n_B = 8$ for the system as described in Section III-A. When ϕ is small, the RIS is near the user, so the RIS-user path is short and the overlap between the BS-RIS and RIS-user blockage regions is large, increasing the joint blocking probability. As ϕ increases, the paths between the BS, RIS, and user get longer and the overlap between the

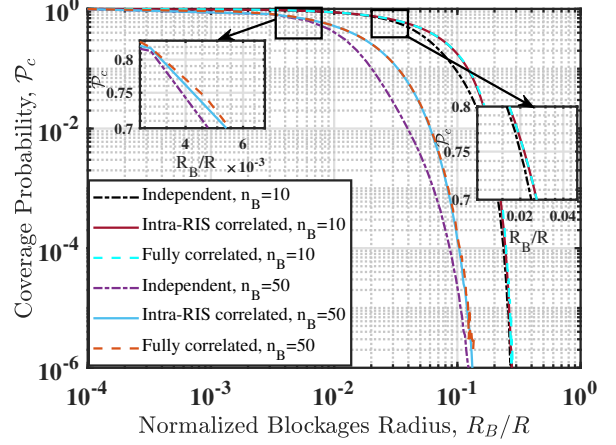


Fig. 7. \mathcal{P}_c versus normalized blockage radius R_B/R for three RIS correlation scenarios: independent, intra-RIS correlated, and fully correlated links, with $R = 50$ m.

two blockage regions gradually reduces, leading to a peak and then a drop in the correlated blocking probability. Near $\phi = \pi$, the RIS is on the opposite side of the user, so the two paths are longest but spatially separate, minimizing their overlap and hence the joint blockage probability. With more blockages in the environment, such as when $n_B = 8$, the overall probability of blockage is higher across all orientations. This indicates that both the RIS orientation and the number of blockages significantly impact the reliability of the BS-RIS-user link. Indeed for fixed user locations, our framework thus provides a strategy to optimally deploy the RISs in a blockage-aware manner.

B. Effect of Blockage Radius on RIS Correlation Models

Fig. 7 illustrates the variation of coverage probability with respect to the normalized blockage size R_B/R , where the system radius is fixed at $R = 50$ m. The results are generated using a Monte Carlo simulation of the exact blockage model. Three blockage correlation models are compared: independent, intra-RIS correlated, and fully correlated. In the intra-RIS correlated model, blockages that affect the links through the same RIS are assumed to be correlated, while links through different RIS remain independent. In the fully correlated model, all links in the system are considered jointly affected by the same blockage events. Two blockage densities are considered: a low density with $n_B = 10$ and a high density with $n_B = 50$. For small blockage sizes, all three models yield high coverage probabilities, and their curves nearly overlap, especially in the zoomed-in regions. In the low-density case, intra-RIS and fully correlated models behave similarly, indicating that correlation has minimal impact under sparse and low-blockage conditions. As the blockage size increases to a moderate level (e.g., $R_B/R = 0.02$ to 0.04), the independent model reports lower coverage probability relative to the correlated models. This is because independent blocking events can block multiple links separately, increasing the chance that at least one link is blocked. In contrast, correlated models may block entire

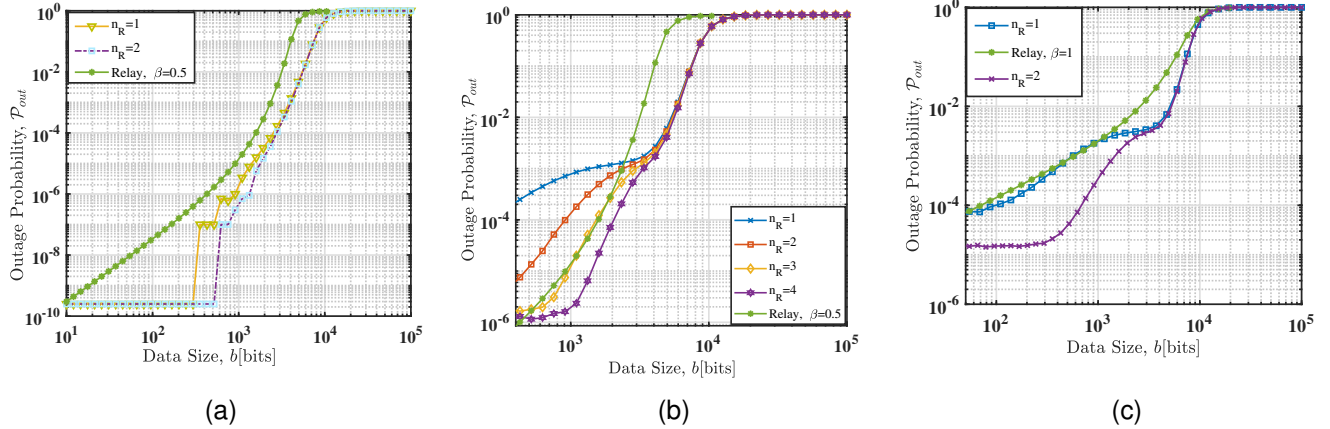


Fig. 8. Comparison plot of the outage probability, P_{out} , versus data size, b , for different numbers of RISs and relays; (a) with the time partitioning factor $\beta = 0.5$, considering $n_B = 0$; (b) with the time partitioning factor $\beta = 0.5$, considering $n_B = 1$ and $R_B = 0.2$ m; (c) with the time partitioning factor $\beta = 1$, considering $n_B = 1$ and $R_B = 0.5$ m, respectively.

groups of links together, preserving some paths and improving coverage. When the blockage size becomes large (e.g., $R_B/R > 0.05$), we observe that the intra-RIS model offers a tractable yet accurate middle ground by capturing correlation among links sharing the same RIS without assuming full dependence. Notably, the deviation between independent and correlated models becomes apparent around $R_B/R \approx 0.025$, especially at high blockage density ($n_B = 50$). This highlights that neglecting blockage correlation can lead to inaccurate performance estimates. Thus, Fig. 7 demonstrates that both blockage density and correlation significantly affect performance, and accurate modeling is essential for evaluating RIS-aided networks under realistic blockage conditions.

C. Effect of the Data Size

In Fig. 8a, we compare the outage probability versus data size for three different schemes: 1) an RIS with $n_B = 0$ (hence, the BS-RIS-user link is always LoS); 2) two RISs with $n_B = 0$ and a network with; 3) relays based on the full coordination strategy as described in [8] with no blockage and the time partitioning factor⁵ $\beta = 0.5$, indicating equal time allocation between the relay and broadcast phases. In all scenarios, the user-RIS-BS link is guaranteed to be in the LoS, as there are no blockages. For low data sizes, the required SNR threshold γ_{th} is relatively low, allowing the RIS to frequently achieve the necessary SNR, which results in a low outage probability. The outage probability with RIS remains almost constant up to moderate data sizes (around $b = 500$ bits), while that of the relay increases gradually even at small data sizes due to its dependence on coordinated transmissions. As data size grows, the required SNR threshold rises, resulting in a steeper increase in outage probability for both RIS and the relay. This confirms that a single RIS outperforms relays when no blockages are present.

Fig. 8b and 8c show the outage probability versus data

sizes when both relays and RIS configurations operate under the same parameters with $R_B = 0.2$ m, $R_B = 0.5$ m, and time partitioning factor $\beta = 0.5$, $\beta = 1$ (broadcast only), respectively. Fig. 8b shows that for smaller data sizes, the relay achieves better coverage and a lower outage probability compared to RIS ($n_R = 1$ and $n_R = 2$, $n_R = 3$ is comparable, and $n_R = 4$ outperform the relay), whereas for larger data sizes, the RIS provides better coverage performance than the relay. At low data sizes, single RIS gives a higher outage probability than the relays due to its passive nature. However, adding more RISs increases the received signal power at the user, reducing the outage probability and narrowing the gap. In Fig. 8b, the outage probability is consistently lower than the relay for all data sizes with 4 RISs. In Fig. 8c, for small b , the $n_R = 2$ RIS configuration achieves lower outage than the broadcast phases, while $n_R = 1$ performs similarly. For large b , the $n_R = 2$ RISs continues to outperform the broadcast phases. This indicates that deploying 2 or 4 RISs can achieve comparable or even better coverage than the relay under these specific conditions, especially when the target data size is large.

D. Effect of the Number of blockages

In Fig. 9, we plot the outage probability as a function of the number of blockages (n_B) for both the RIS configurations (with $\beta = 1$), and for the relay under two different time partitioning factors $\beta = 0.5$ and $\beta = 1$. For small n_B , the user-RIS-BS link remains in LoS, ensuring better coverage and low outage probability. As n_B increases, the likelihood of blockages blocking the BS-RIS-user link rises, leading to higher outage probability. However, at high n_B , the outage probability saturates since additional blockages have minimal effect once the link is already blocked. With relays, the outage probability increases more gradually, whereas for RIS, it rises sharply due to the lack of signal amplification. As a result, the RIS curve is steeper than the relay scenario. A single RIS plot shows a higher outage probability compared to the relays. However, as the number of RIS increases, the plot starts to

⁵ β controls the time split between the broadcast and relaying phases for the relay link. For the RIS, which passively reflects the signal without forwarding, we have $\beta = 1$.

flatten or decrease in the outage probability. In Fig. 9, the outage probability is consistently lower than that of the relay with $\beta = 1$ or surpasses the relay with 6 RISs, whereas the relay with $\beta = 0.5$ is observed for 7 RISs.

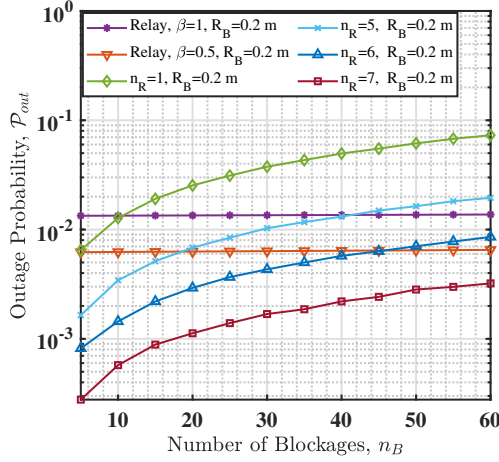


Fig. 9. Comparison plot of the outage probability, P_{out} , versus the number of blockages, n_B , for different numbers of RISs ($n_R = 1, 5, 6, 7$), $R = 200m$ and $R_B = 0.2m$ with relays at $\beta = 0.5$ and $\beta = 1$.

E. Effect of the Radius of the Deployment Region

Fig. 10 illustrates the outage probability P_{out} as a function of the warehouse radius R for three scenarios: (a) a fixed low number of blockages ($n_B = 2$), (b) a fixed high number of blockages ($n_B = 8$), and (c) a constant blockage density λ_B , for different values of n_R . For smaller values of R , the blockages are relatively denser within the room, resulting in a higher outage probability. As R increases, the blockage density decreases, which leads to a reduction in the outage probability until a critical point is reached. Beyond this point, further increases in R cause the outage probability to rise due to the reduction in signal power caused by the larger distance between the RISs and the user. In Fig. 10a, when $n_B = 2$, the outage probability gradually decreases for $n_R = 1, 2, 4$, & 8. The critical point at which the outage probability starts to increase depends on the number of RISs. For instance, the critical point occurs at approximately $R = 100$ m for $n_R = 1$, around $R = 120$ m for $n_R = 2$, $R = 140$ m for $n_R = 4$, and $R = 180$ m for $n_R = 8$. This indicates that deploying more RISs allows the network to sustain low outage probabilities even as the warehouse deployment region increases. In Fig. 10b, for a higher number of blockages ($n_B = 8$), a similar trend is observed, but with higher overall outage levels due to the increased probability of link blockage.

In Fig. 10c, we consider the case when the warehouse radius increases but the blockage density $\lambda_B = \frac{n_B}{\pi R_{ref}^2}$ is kept constant by scaling $n_B \propto R^2$. In this case, the outage probability typically increases with the deployment radius R . This is because larger areas lead to greater distances between the BS, RISs, and the user, which increases the chance of blockages. The figure also shows that deploying more RIS nodes (e.g., $n_R = 8$) improves reliability, particularly in moderate-sized

environments. However, as R grows, even multiple RISs become less effective due to the rising number of blockages. This highlights that outage performance is influenced not only by blockage density but also by the overall coverage area and the separation between devices. Therefore, in large-scale or densely obstructed deployments, RIS-assisted communication systems must be carefully scaled in accordance with both the deployment range and the expected blockage intensity to maintain reliable performance.

F. Effect of the Size of the Blockages

In Fig. 11, we plot the outage probability as a function of the radius of the blockages R_B for different values of n_R . The plot shows an increasing trend as R_B increases. This is because the larger blockages are more likely to block the path between the RIS, the BS, and the user. When $n_R = 1$, the outage probability is low for small values of R_B and increases for higher values of R_B . The outage probability is low at $R_B = 1$ m and high at $R_B = 10$ m. When we add more RISs, the trend of the plot is the same, but the outage probability is lower compared to a single RIS because the RISs can reflect the signal around the blockages. For $n_R = 1$, the outage probability is 10 times greater than for $n_R = 8$ when the size of the blockages is small. However, as the size of the blockage increases, the ratio of the outage probability gradually decreases.

G. Effect of the Number of RISs

The plot in Fig. 12 illustrates the impact of the number of RISs (n_R) on the outage probability (P_{out}) for different values of n_B . Across all values of n_B , increasing the number of RISs leads to a significant reduction in P_{out} , confirming the effectiveness of RIS deployment in enhancing link reliability. For smaller values of n_B (e.g., $n_B = 10$ or 50), the outage probability drops sharply with just a few RISs, quickly approaching negligible values. This indicates that even minimal RIS deployment can yield substantial performance improvements in sparse environments. For intermediate values (e.g., $n_B = 100$ and $n_B = 200$), the decrease is still significant, but slightly more RISs are required to reach very low outage levels. In contrast, for larger values of n_B (e.g., $n_B = 300$ or 500), the decrease in outage probability becomes more gradual, with P_{out} remaining above 10^{-5} even with 10 RISs in the $n_B = 500$ case. This highlights that higher blockage density or complexity requires more RISs to achieve comparable reliability. Furthermore, most curves exhibit a saturation trend, where adding more RISs beyond a certain point yields diminishing returns. These results imply that the effectiveness of RIS deployment is strongly influenced by the system configuration, and careful optimization of RIS quantity is necessary, particularly in scenarios with high n_B , to meet reliability requirements efficiently. Therefore, strategic planning of RIS deployment is essential to balance performance with deployment costs, especially in complex environments.

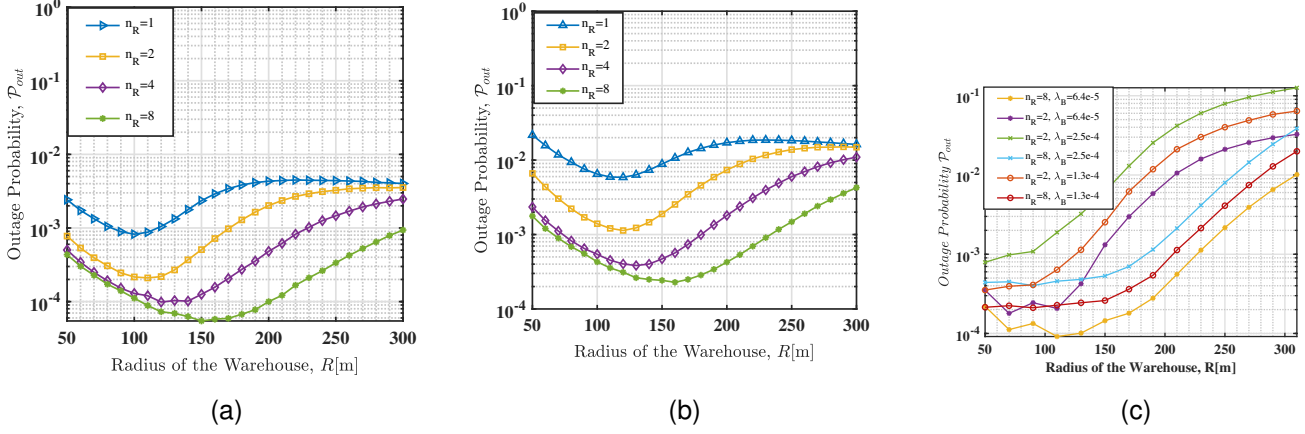


Fig. 10. Outage probability, P_{out} , versus warehouse radius for different numbers of RISs, (a) a fixed low number of blockages ($n_B = 2$), (b) a fixed high number of blockages ($n_B = 8$), and (c) constant blockage density $\lambda_B = 6.5 \times 10^{-5}$, 1.3×10^{-4} , and 2.5×10^{-4} with $R_{ref} = 100$ m, respectively.

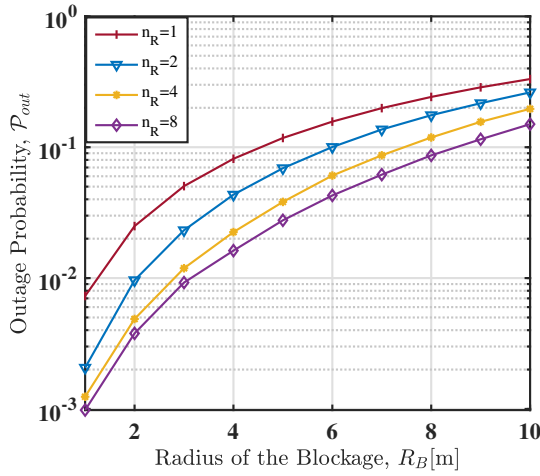


Fig. 11. Outage probability, P_{out} , versus the radius of the Blockages (R_B [m]), for different numbers of RISs ($n_R = 1, 2, 4, 8$), where $n_B = 4$ and $R = 100$ m.

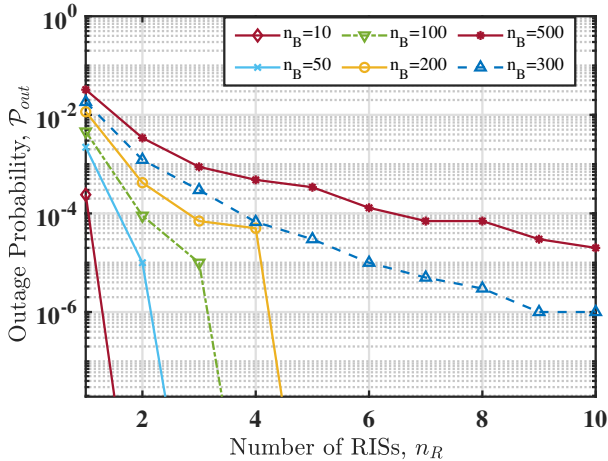


Fig. 12. Variation of the outage probability, P_{out} , versus the number of RISs, n_R , for different numbers of blockages ($n_B = 10, 50, 100, 200, 300, 500$), $R = 100$ m and $R_B = 0.2$ m.

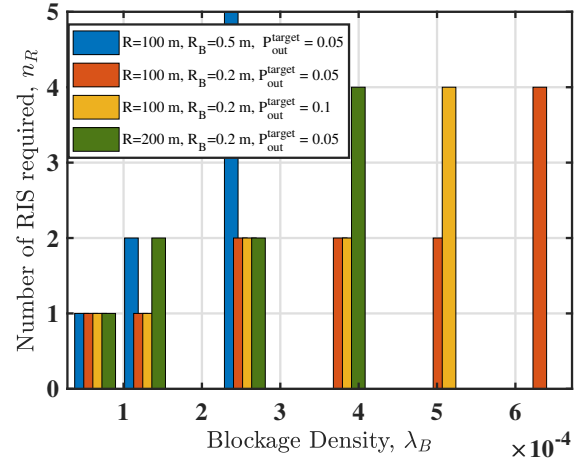


Fig. 13. Minimum number of RISs, n_R , required versus blockage density, λ_B , for outage probability targets $P_{out}^{target} = 0.05$ and 0.1 , under varying warehouse radii ($R = 100$ m, 200 m) and blockage sizes ($R_B = 0.2$ m, 0.5 m).

H. Number of RISs Required Under Outage Probability Constraint

Fig. 13 shows the minimum number of RISs (n_R) needed to meet a target outage probability (P_{out}^{target}) for different blockage densities (λ_B). As λ_B increases, more RISs are required to overcome link blockages and maintain outage performance. For example, when comparing scenarios with the same deployment radius R and the target outage probability P_{out}^{target} but different blockage sizes (e.g., $R_B = 0.2$ m vs. $R_B = 0.5$ m), the case with the larger blockage radius consistently requires more RISs across all values of λ_B . This is because larger blockages occupy more area and are more likely to obstruct communication links. The influence of the outage probability target is also evident. A more relaxed requirement (e.g., $P_{out}^{target} = 0.1$ instead of 0.05) permits fewer RISs to be deployed, as the system can tolerate a higher probability of link failure. Moreover, increasing the deployment radius (e.g., $R = 200$ m vs. $R = 100$ m) results in a greater RIS requirement. This is due to both increased link distances and a

fixed blockage density λ_B , the expected number of blockages grows with the area, specifically, by a factor of four when R doubles. As a result, the blockage environment becomes more severe with increasing R , necessitating the addition of more RISs to maintain reliable coverage. Therefore, the figure highlights that the blockage size, area dimensions, and the outage probability significantly influence RIS deployment, emphasizing the need for careful system design in blockage-prone environments where reliable connectivity is critical.

VI. CONCLUSIONS

Placing RISs too close or too far from the BS increases the likelihood of simultaneous blockages in the BS-RIS and RIS-user links, which degrades link reliability. In this paper, we extended the analysis to networks with multiple RISs under realistic blockage conditions by incorporating intra- and inter-link correlation models. We derived closed-form expressions for LoS/NLoS probabilities and outage probability, revealing how blockage characteristics and user location influence coverage. For a single RIS, outage probability increases sharply with blockage density, and we show that beyond a critical number of blockages, traditional relays can outperform a single RIS. However, we demonstrated that deploying multiple RISs can effectively restore and enhance network performance, offering a scalable solution to combat severe blockage. Our study also shows that assuming independent blockages may lead to inaccurate predictions when obstructions are large, highlighting the importance of accounting for blockage correlation in the system model. Finally, we analyzed the effect of warehouse size and blockage density on rate coverage, identifying practical design thresholds where RISs can outperform relaying-based solutions. These findings provide useful insights for practical deployment of reliable, low-latency RIS-aided IIoT networks capable of meeting stringent URLLC requirements.

REFERENCES

- [1] G. Cena *et al.*, "Hybrid wired/wireless networks for real-time communications," *IEEE Ind. Electron. Mag.*, vol. 2, no. 1, pp. 8–20, 2008.
- [2] V. C. Gungor and G. P. Hancke, "Industrial wireless sensor networks: Challenges, design principles, and technical approaches," *IEEE Trans. Ind. Electron.*, vol. 56, no. 10, pp. 4258–4265, 2009.
- [3] Z. Li, M. A. Uusitalo, H. Shariatmadari, and B. Singh, "5g urllc: Design challenges and system concepts," in *Proc. international symposium on wireless communication systems (ISWCS)*, pp. 1–6, IEEE, 2018.
- [4] S. Tayeb, S. Latifi, and Y. Kim, "A survey on iot communication and computation frameworks: An industrial perspective," in *Proc. annual Computing and Communication Workshop and Conference (CCWC)*, pp. 1–6, IEEE, 2017.
- [5] S. W. H. Shah, A. N. Mian, S. Mumtaz, M. Wen, T. Hong, and M. Kadoch, "Protocol stack perspective for low latency and massive connectivity in future cellular networks," in *Proc. IEEE International Conference on Communications (ICC)*, pp. 1–7, IEEE, 2019.
- [6] M. Cheffena, "Industrial wireless communications over the millimeter wave spectrum: opportunities and challenges," *IEEE Communications Magazine*, vol. 54, no. 9, pp. 66–72, 2016.
- [7] V. N. Swamy *et al.*, "Cooperative communication for high-reliability low-latency wireless control," in *Proc. IEEE ICC*, pp. 4380–4386, 2015.
- [8] G. Ghatak *et al.*, "Stochastic geometry framework for ultrareliable cooperative communications with random blockages," *IEEE J. Internet Things*, vol. 9, no. 7, pp. 5150–5161, 2021.
- [9] X. Mu, Y. Liu, L. Guo, J. Lin, and R. Schober, "Intelligent reflecting surface enhanced indoor robot path planning: A radio map-based approach," *IEEE Trans. Wirel. Commun.*, vol. 20, no. 7, pp. 4732–4747, 2021.
- [10] R. Jurdi, S. R. Khosravirad, and H. Viswanathan, "Variable-rate ultra-reliable and low-latency communication for industrial automation," in *Proc. IEEE Annual Conference on Information Sciences and Systems (CISS)*, pp. 1–6, 2018.
- [11] N. Brahmhi, O. N. Yilmaz, K. W. Helmersson, S. A. Ashraf, and J. Torsner, "Deployment strategies for ultra-reliable and low-latency communication in factory automation," in *2015 IEEE Globecom Workshops (GC Wkshps)*, pp. 1–6, IEEE, 2015.
- [12] J. G. Andrews *et al.*, "Modeling and analyzing millimeter wave cellular systems," *IEEE Trans. Commun.*, vol. 65, no. 1, pp. 403–430, 2016.
- [13] T. Bai and R. W. Heath, "Coverage and rate analysis for millimeter-wave cellular networks," *IEEE Trans. Wirel. Commun.*, vol. 14, no. 2, pp. 1100–1114, 2014.
- [14] T. Bai, R. Vaze, and R. W. Heath, "Analysis of blockage effects on urban cellular networks," *IEEE Trans. Wirel. Commun.*, vol. 13, no. 9, pp. 5070–5083, 2014.
- [15] F. Okta *et al.*, "Blockage Effects in RIS-enabled Communication," in *Proc. Int. Balkan Conf. Commun. Netw. (BalkanCom)*, pp. 1–6, 2023.
- [16] S. K. Gupta *et al.*, "Impact of blocking correlation on the performance of mmwave cellular networks," *IEEE Trans. Commun.*, vol. 70, no. 7, pp. 4925–4939, 2022.
- [17] G. Ghatak *et al.*, "Where to deploy reconfigurable intelligent surfaces in the presence of blockages?," in *Proc. IEEE PIMRC*, pp. 1419–1424, 2021.
- [18] A. K. Gupta *et al.*, "Macrodiversity in cellular networks with random blockages," *IEEE Trans. Wirel. Commun.*, vol. 17, no. 2, pp. 996–1010, 2017.
- [19] E. Hriba and M. C. Valenti, "Correlated blocking in mmwave cellular networks: Macrodiversity, outage, and interference," *Electronics*, vol. 8, no. 10, p. 1187, 2019.
- [20] S. Aditya, H. S. Dhillon, A. F. Molisch, and H. M. Behairy, "A tractable analysis of the blind spot probability in localization networks under correlated blocking," *IEEE Transactions on Wireless Communications*, vol. 17, no. 12, pp. 8150–8164, 2018.
- [21] A. Samuylov, M. Gapeyenko, D. Moltchanov, M. Gerasimenko, S. Singh, N. Himayat, S. Andreev, and Y. Koucheryavy, "Characterizing spatial correlation of blockage statistics in urban mmwave systems," in *2016 IEEE Globecom Workshops (GC Wkshps)*, pp. 1–7, IEEE, 2016.
- [22] F. Baccelli and X. Zhang, "A correlated shadowing model for urban wireless networks," in *2015 IEEE Conference on Computer Communications (INFOCOM)*, pp. 801–809, IEEE, 2015.
- [23] M. Di Renzo, A. Zappone, M. Debbah, M.-S. Alouini, C. Yuen, J. De Rosny, and S. Tretyakov, "Smart radio environments empowered by reconfigurable intelligent surfaces: How it works, state of research, and the road ahead," *IEEE journal on selected areas in communications*, vol. 38, no. 11, pp. 2450–2525, 2020.
- [24] Ö. Özdogan *et al.*, "Intelligent reflecting surfaces: Physics, propagation, and pathloss modeling," *IEEE Wirel. Commun. Lett.*, vol. 9, no. 5, pp. 581–585, 2019.
- [25] J. Ye, A. Kammoun, and M.-S. Alouini, "Spatially-distributed ris vs relay-assisted systems: A fair comparison," *IEEE Open Journal of the Communications Society*, vol. 2, pp. 799–817, 2021.
- [26] M. A. Kishk and M.-S. Alouini, "Exploiting randomly located blockages for large-scale deployment of intelligent surfaces," *IEEE J. Sel. Areas Commun.*, vol. 39, no. 4, pp. 1043–1056, 2020.
- [27] Z. Li *et al.*, "RIS-assisted mmWave networks with random blockages: Fewer large RISs or more small RISs?," *IEEE Trans. Wirel. Commun.*, vol. 22, no. 2, pp. 986–1000, 2022.
- [28] H. Ren *et al.*, "Average data rate and decoding error probability analysis for ris-aided urllc in a factory automation scenario," in *Proc. IEEE/CIC Int. Conf. Commun. China (ICCC Workshops)*, pp. 177–182, 2021.
- [29] J. Kokkonen and M. Juntti, "Stochastic geometry based interference analysis of multiuser mmWave networks with RIS," in *Proc. IEEE PIMRC*, pp. 567–572, 2021.
- [30] M. H. Samuh, A. M. Salhab, and A. H. A. El-Malek, "Performance analysis and optimization of ris-assisted networks in nakagami-m environment," *arXiv preprint arXiv:2010.07841*, 2020.
- [31] G. Sun, F. Baccelli, K. Feng, L. U. Garcia, and S. Paris, "A stochastic geometry framework for performance analysis of ris-assisted ofdm cellular networks," *arXiv preprint arXiv:2310.06754*, 2023.
- [32] J. Gil-Pelaez, "Note on the inversion theorem," *Biometrika*, vol. 38, no. 3-4, pp. 481–482, 1951.